Author's preprint version of the article:

Analysis of Major Air Pollutants and Submicron Particles in New York City and Long Island

Masiol, M., Hopke, P.K., Felton, H.D., Frank, B.P., Rattigan, O.V., Wurth, M.J., LaDuke, G.H.

The original paper is available at:

https://www.sciencedirect.com/science/article/pii/S1352231016308500

ANALYSIS OF MAJOR AIR POLLUTANTS AND SUBMICRON PARTICLES IN NEW YORK CITY AND LONG ISLAND

M. Masiol,[1] P. K. Hopke,[1] H.D. Felton,[2] B.P. Frank,[2] and O.V. Rattigan[2]

[1] Center for Air Resources Engineering and Science, Clarkson University, Potsdam, NY 13699
[2] NYS Department of Environmental Conservation, Division of Air Resources, BAQS, Albany NY 12233-3256

HIGHLIGHTS

> One-year air quality data measured hourly at 2 urban sites in NYC and Long Island

> Particle number resolved over 6 bins, gases, PM2.5 mass, EC/OC and sulfate measured

> Primary and secondary organic carbon are estimated using the EC tracer method

> Seasonal, weekly, diurnal cycles and relationships with weather are investigated

> Location of the potential sources and role of regional transport are discussed

Analysis of Major Air Pollutants and Submicron Particles in New York City and Long Island

M. Masiol,[1] P. K. Hopke,[1] H.D. Felton,[2] B.P. Frank,[2] and O.V. Rattigan[2]

[1] Center for Air Resources Engineering and Science, Clarkson University, Potsdam, NY 13699
[2] NYS Department of Environmental Conservation, Division of Air Resources, BAQS, Albany NY 12233-3256

Abstract

A year-long sampling campaign of major air pollutants and submicron particle number size distributions was conducted at two sites taken as representative of city-wide air quality in New York City and Long Island, respectively. A number of species were quantified with hourly time resolution, including particle number concentrations in 6 size ranges (20-30 nm, 30-50 nm, 50-70 nm, 70-100 nm, 100-200 nm, and >200 nm), nitrogen oxides, sulfur dioxide, ozone, carbon monoxide, methane, non-methane hydrocarbons, $PM_{2.5}$ mass concentration and some PM major components (sulfate, organic and elemental carbon). Hourly concentrations of primary and secondary organic carbon were estimated using the EC tracer method. Data were matched with weather parameters and air parcel back-trajectories. A series of tools were thus applied to: (i) study the seasonal, weekly, diurnal cycles of pollutants; (ii) investigate the relationships amongst pollutants through correlation and lagged correlation analyses; (iii) depict the role of atmospheric photochemical processes; (iv) examine the location of the potential sources by mean of conditional bivariate probability function analysis and (v) investigate the role of regional transport of air masses to the concentrations of analyzed species. Results indicate that concentrations of NO_x, SO_2, CO, non-methane hydrocarbons, primary OC and EC are predominantly determined by local sources, but are also affected by regional transports of polluted air masses. On the contrary, the transport of continental polluted air masses has a main effect in raising the concentrations of secondary $PM_{2.5}$ (sulfate and secondary organic carbon). By providing direct information on the concentrations and trends of key pollutants and submicron particle number concentrations, this study finally enables some general considerations about air quality status and atmospheric processes over the New York City metropolitan area.

1.   INTRODUCTION

Over the last several decades, an increasing number of epidemiologic studies have concluded that ambient air pollution and particularly airborne particulate matter (PM) are causal risk factors for many adverse human health effects, including respiratory illnesses (Götschi et al., 2008; Laumbach and Kipen, 2012; Adam et al., 2015), cardiovascular diseases (Anderson et al., 2012; Shah et al., 2013; Franklin et al., 2015) and carcinogenic effects (Turner et al., 2011; Pope et al., 2011; Loomis et al., 2013). Given the biological evidence, outdoor air pollution and airborne particulate matter (PM) have been categorized in class 1 by the International Agency for Research on Cancer in 2013, i.e. known carcinogenic to human beings (Straif et al., 2013).

A significant drop in the ambient concentrations of many air pollutants has been measured in many developed countries (including U.S.) as a result of implementation of legislation and regulations through the application of successful abatement technologies and other mitigation measures (Parrish et al., 2011; Colette et al, 2011). Current United States air quality is regulated through the National Ambient Air Quality Standards (NAAQS) that set limit values to be attained across U.S. for pollutants considered harmful to public health and the environment, i.e. nitrogen dioxide (NO_2), ozone (O_3), sulfur dioxide (SO_2), carbon monoxide (CO), PM with aerodynamic diameters less than 10 and 2.5 μm (PM_{10} and $PM_{2.5}$, respectively) and particle-bound lead.

New York City (NYC) is the most populous city in the U.S. with ~8.5 million inhabitants in 2014. However, the population reaches almost 20 million inhabitants when considering the whole New York–New Jersey–Pennsylvania metropolitan area. Air quality has generally improved since 1970s across NYC (NYC Department of Health and Mental Hygiene, 2013a). For example, Parrish et al. (2011) have reported slow improvements for both ozone and $PM_{2.5}$ between 2000 and 2010, while Duncan et al. (2016) have observed a strong decrease (-45.5%) in NO_2 from 2005 to 2014. Downward trends in air pollutants across New York were observed by Buckley and Mitchell (2011), while substantial decreases in $PM_{2.5}$ mass and major components across New York since the early 2000s were reported by Rattigan et al. (2016). Currently, NAAQS are generally not exceeded in NYC (NY State Dep. Environmental Conservation, 2016), except for ozone (marginal to moderate non-attainment). However, air pollution still remains a serious concern for policy-makers and the scientific community in NYC as well as in

64   the whole metropolitan area. Even with attainment of the NAAQS, it has been estimated that

65   ambient concentrations of $PM_{2.5}$ still contribute to more than 3000 deaths every year, 2000

66   hospital admissions for lung and heart conditions, and approximately 6000 emergency

67   department visits for asthma in children and adults (NYC Department of Health and Mental

68   Hygiene, 2013a;b).

69   Despite the number of stations measuring air quality and the large number of scientific

70   studies available in literature, limited data are still available for some air pollutants, including

71   submicron particles (SMPs, <1 μm) and ultrafine particles (UFPs, less than 100 nm in diameter),

72   which have been widely associated with severe adverse effects upon human health (e.g., Knibbs

73   et al., 2011; Strak et al., 2012; Ostro et al., 2015; Lanzinger et al., 2016). Moreover, limited

74   studies have focused on air pollution climate, i.e. on the relationships amongst air pollutants and

75   weather.

76   This study investigates air pollutions in NYC and Long Island through the analysis of

77   hourly-resolved concentrations of common gaseous air pollutants, $PM_{2.5}$ mass and $PM_{2.5}$-bound

78   major species, submicron particle number concentrations and their size distributions, with special

79   emphasis for UFPs. Intensive sampling campaigns were simultaneously conducted at two sites:

80   Queens (NYC) and Eisenhower Park (Long Island). A large set of air pollutants was measured

81   over 1 year (2009-2010) at 1 h intervals. Datasets include: (i) key gaseous air pollutants, i.e.

82   nitrogen oxides ($NO+NO_2 \equiv NO_x$), sulfur dioxide (SO_2), ozone (O_3), carbon monoxide (CO),

83   methane (CH_4), non-methane hydrocarbons (NMHCs), total hydrocarbons (THCs); (ii) $PM_{2.5}$

84   mass and $PM_{2.5}$-bound species, such as sulfate (SO_4^{2-}), organic (OC), elemental (EC) and total

85   (TC) carbon; (iii) particle number concentrations (PNC) over 6 size ranges (20-30 nm, 30-50 nm,

86   50-70 nm- 70-100 nm, 100-200 nm, and 200 to ~1000 nm). The seasonal, weekly, and diurnal

87   cycles of the air pollutants were investigated in detail along with several derived variables. The

88   concentrations of primary and secondary organic carbon were estimated using an EC tracer

89   method. Data were matched with micro-meteorological parameters and analyzed to explore the

90   possible effects of weather upon the air quality and to locate the probable local emission sources.

91   A back-trajectory-based hybrid model was applied for assessing the potential role of regional and

92   long-range transports upon air quality. These results give important insights into pollutant

93   sources, influences upon concentrations and key inter-relationships in pollutant behaviors and

94 presents a synthesized description of pollution climate regimes for typical urban sites in NYC or

95 even for large cities across northeastern U.S.

96

97 **2.   MATERIALS AND METHODS**

98 **2.1   Site description**

99 Measurements were made from June 2009 to July 2010 at two sites categorized as urban, i.e.

100 representative of city-wide background pollution concentrations. Queens College (QC: 40°

101 44.225'N; 73° 49.295'W; 24 m a.s.l.) is located in a high population density section of Queens

102 County (Figure 1) and it is representative of the New York City metropolitan area. QC is also

103 affected by emissions from two traffic highways, i.e. the Long Island Expressway (I-495) and the

104 Van Wyck Expressway (I-678). Eisenhower Park (EP: 40° 44.586'N 73° 35.132'W; 25 m a.s.l.)

105 is situated on the border of a 3.8 km^2-wide public park located in Nassau County. The park is

106 devoted to many entertainment and sport activities and is backed by unoccupied parklands.

107 However, EP is also affected by: (i) heavy road traffic as it is adjacent to a 4 lane roadway that

108 runs parallel to the site in a NNW direction, within 22 m of a roadway in a W-WSW direction,

109 and within 53 m of the roadway in a S direction; and (ii) emissions from a waste-to-energy

110 conversion plant and from several restaurants close to the site (Figure 1).

111

112 **2.2   Experimental**

113   Instruments were operated continuously over the sampling period to quantify ambient

114 air pollutant concentrations with 1 h resolution time. A more extensive range of pollutants were

115 monitored at QC (NO, NO_2, NO_x, SO_2, O_3, CO, CH_4, NMHCs, THC, $PM_{2.5}$, SO_4^{2-}, OC, EC, opt.

116 EC, TC and SMP) than at EP (NO, NO_2, NO_x, SO_2, $PM_{2.5}$ and SMP).

117   Two ultrafine particle monitors (TSI Model 3031) were deployed at both sites to

118 measure particle size distributions from 20 nm (electrical mobility diameter) to approximately

119 $PM_{2.5}$ μm in six channels: 20-30 nm (ch1), 30-50 nm (ch2), 50-70 nm (ch3), 70-100 nm (ch4),

120 100-200 nm (ch5) and >200 nm (ch6). The instruments operated with $PM_{2.5}$ cyclones, i.e. the

121 upper size was set to particles with an aerodynamic diameter less than 2.5 μm. The operating

122 principle of the UFP monitor is based diffusion charging of particles using a "Corona-Jet"

123   charger (Medved et al., 2000), followed by size segregation in a differential mobility analyzer

124   and detection via a sensitive electrometer.

125   U.S. EPA equivalent or reference methods were used for the gas measurements

126   (Thermo Electron Corporation model 42C $NO-NO_2-NO_x$; model 43C SO_2; model 49C O_3; model

127   48C CO). Methane, Non-Methane Hydrocarbons (NMHCs), and total hydrocarbons (THC) were

128   analyzed using flame ionization detector method (model APHA-360, HORIBA Ltd., Japan).

129          $PM_{2.5}$ mass concentrations were measured with tapered element oscillating

130   microbalances (Thermo-Fisher Scientific TEOM 1400ab) with 2.5 μm cut size inlets. However, a

131   TEOM-FDMS system was deployed at QC, while a simple TEOM was used at EP. The main

132   concern with the use of the simple TEOM technique is the loss of the more volatile component

133   (principally some semi-volatile hydrocarbons and nitrates) because the inlet is held at a

134   temperature ~50°C. A non-linear Julian Day based adjustment was thus applied to the TEOM

135   data: it removes much of the seasonal bias and gives approximate comparability with the Federal

136   Reference Method (FRM). Details are reported in Felton (2005).

137   Particulate sulfate was determined with a sulfate analyzer (Thermo Scientific model

138   5020i), while particulate carbonaceous components (OC, EC, TC) were quantified by a semi-

139   continuous carbon aerosol analyzer (Sunset Lab., Tigard, OR, USA) operating a modified

140   NIOSH 5040 thermo-optical protocol on an hourly sample collection similar to Bauer et al.

141   (2009). For EC, both the thermal (EC) and "black" optical EC (opt. EC at 632 nm) were

142   quantified.

143

144   **2.3   Weather data and meteorology-based models**

145   Ambient air temperature, wind speed and direction, relative humidity (RH) and

146   atmospheric pressure were recorded hourly at weather stations which were chosen as

147   representative of the average weather conditions across the study area: LaGuardia and Republic

148   airports, respectively, for QC and EP. Since no direct solar radiation (SR) data were available at

149   the weather stations, the total direct and diffuse SR (METSTAT-modeled) was retrieved from the

150   National Solar Radiation Database (NREL, 2012).

151   Conditional probability function (CPF) analysis is widely used to locate the potential

152   local sources affecting a site. It is performed by matching wind direction data with air pollutants

153   concentrations (Kim et al., 2003; Pekney et al., 2006; Kara et al., 2015). More recently, this

154   approach was extended to the bivariate case to produce a conditional bivariate probability

155   function (CBPF) plots using wind speed as a third variable plotted on the radial axis: details of

156   the method are provided in Uria-Tellaetxe and Carslaw (2014). Essentially, CBPF assesses the

157   probability that a source contribution from a given wind direction/speed sector exceeds a

158   predetermined threshold criterion (concentrations >75th percentile, in this case). This approach

159   was used to identify the most probable local emission sources.

160   Back-trajectories were computed by the NOAA/ARL hybrid single particle Lagrangian

161   integrated trajectory (HYSPLIT4) model (Stein et al., 2015; Rolph, 2016) from the

162   NCEP/NCAR Reanalysis data. The HYSPLIT parameters were set as -96 h run time with a

163   starting height of 500 m a.g.l. The potential source contribution function (PSCF) (Ashbaugh et

164   al., 1985; Lee and Hopke, 2006; Hopke, 2016) was used to identify regional scale source

165   locations. PSCF calculates the conditional probability that a source is located at latitude i and

166   longitude j as:

167    $$PSCF = \frac{m_{i,j}}{n_{i,j}}, \tag{1}$$

168   where $n_{i,j}$ is the number of times the trajectory endpoints fell into the i,j-th cell in the domain

169   grid, and $m_{i,j}$ represents the number of times the concentrations exceed a threshold

170   (concentrations >75th percentile, in this case). The cells with high PSCF probabilities indicate a

171   likely source location. Since cells with few data may bias the results, a weighting factor is

172   applied to reduce their effect. The details are provided in Polissar et al. (2001).

173   Data were analyzed using R version 3.2.2 (R Development Core Team, 2008) and a

174   series of packages including 'openair' (Carslaw and Ropkins, 2012). Details of polar plot

175   analysis shown in this study are given in Carslaw et al. (2006) and Uria-Tellaetxe and Carslaw

176   (2014).

177

178

179   **3   RESULTS**

180   Annual concentrations of measured pollutants at the two sites (all available data recorded during

181   the whole study period) are given as box and whisker plots (Figure 2). On average, results show

182   that gaseous species measured at both sites have similar concentrations, following the order (in

183   ppb) NO_x (28.9 and 24.5 in QC and EP, respectively)> NO_2 (19.6, 14.3)> NO (9.4, 10.3)> SO_2

184   (2.8, 2.3). Average $PM_{2.5}$ mass concentrations were 10 and 9.4 $\mu g\ m^{-3}$ at QC and EP,

185   respectively, while total SMPs averaged 8209 and 7596 particles cm^{-3}. The size distributions

186   show the highest concentrations in the 30-50 nm range at both sites, followed by 20-30 nm.

187   Particles >200 nm had the lowest concentrations. QC experiences higher concentrations for all of

188   the measured air pollutants, except for NO.

189   At QC, annual $PM_{2.5}$ mass concentrations are dominated by sulfate (20.9%) and OC

190   (20.6%), with EC accounting for 6.5%. Assuming the sulfate is fully neutralized by ammonia

191   and a OM/OC ratio in the range of 1.9–2.1, as reported for atmospheric aerosols sampled at the

192   Pittsburgh supersite (Polidori et al., 2008), ammonium sulfate accounts for ~25% of total $PM_{2.5}$

193   mass (2.7 $\mu g\ m^{-3}$), while organic matter represents 39-43% (4-5 $\mu g\ m^{-3}$).

194   Additional variables were calculated and the results are shown in Figure 2. The

195   NO_2/NO_x ratio indicates the complex photochemistry in the $NO-NO_2-O_3$ system. NOx emissions

196   from combustion is primarily NO (~90%) and rapidly reacts with O_3 and radicals to form NO_2

197   (Jenkin and Hayman, 2000; Finlayson Pitts and Pitts, 2000; Seinfeld and Pandis, 2006). Annual

198   average NO_2/NO_x ratios were found around 0.8 (0.82 at QC and 0.77 at EP). Total oxidant

199   concentration ($OX=O_3+NO_2$) was calculated as an indirect estimation of the atmospheric

200   oxidative potential (Kley et al., 1999). At QC, annual average OX concentrations were 43 ppb,

201   of which ozone contributed for 54% and NO_2 for the remaining 46%. The sulfate/SO_2 ratio may

202   give important insights upon the degree of SO_2 oxidation and on the consequent speciation of

203   sulfur into the two species (Stockwell and Calvert, 1983; Stockwell, 1994). Sulfate accounts for

204   30–60% of monthly average $PM_{2.5}$ mass in the East U.S. (Hand et al., 2012a;b). The sulfate/SO_2

205   ratio was calculated over the mass concentrations normalized for their sulfur content: i.e.

206   converting SO_2 to $\mu g\ m^{-3}$ and dividing the species by the respective molecular weights. Annual

207   average of sulfate/SO_2 ratio at QC was 0.4. This value indicates that the atmospheric sulfur is

208   primarily oxidized S(IV).

209

210   **3.1   Primary and secondary organic carbon**

211   Primary (OC_{pri}) and secondary (OC_{sec}) organic carbon aerosols are important bulk constituents of

212    $PM_{2.5}$. Secondary OC is formed in the atmosphere from the oxidation of volatile organic

213   compounds (VOCs) of both biogenic (e.g., Lane and Pandis, 2007; Brown et al., 2009) and

214   anthropogenic (e.g., Ng et al., 2007; Henze et al., 2008; Donahue et al., 2009) origins. It was

215   estimated that OC_{sec} accounts for about 35-77% of total OC across the continental U.S. (Yu et

216   al., 2004; Cabada et al., 2004a; Yu et al., 2007; de Gouw et al., 2008). In this study, a widely

217   used EC tracer method is applied to estimate the partitioning between OC_{pri} and OC_{sec} using

218   hourly resolved OC and EC data collected at QC. Briefly, since EC is a primary pollutant, the

219   adopted empiric method assumes that OC_{pri} is dependent from EC:

220     $$OC_{pri} = EC \cdot \left[\frac{OC}{EC}\right]_{pri} + b \qquad (2)$$

221   where OC/EC_{pri} is the ratio for the primary sources affecting the site and b includes the non-

222   combustion contribution to OC_{pri} and sampling artifacts (Turpin and Huntzicker, 1995; Strader et

223   al., 1999; Lim and Turpin, 2002; Cabada et al., 2004a). Subsequently, OC_{sec} can be finally

224   assessed as:

225     $$OC_{sec} = OC - OC_{pri} \qquad (3)$$

226   The limitations and the uncertainties associated with EC tracer methods have been noted (e.g.,

227   Day et al., 2015) and are mainly related to OC/EC_{pri}. This basic method relies on the ability to

228   isolate periods which are dominated by primary EC and OC, i.e. low photochemical secondary

229   organic aerosol (SOA) production. It assumes that primary EC and OC are derived from similar

230   sources and exhibit similar temporal patterns throughout the year. The $(OC/EC)_{pri}$ value is rarely

231   measured experimentally and, thus, needs to be estimated. A scatterplot of OC versus EC

232   concentrations for all samples and for samples selected by adopting criteria similarly to Cabada

233   et al. (2004a) is shown in Figure SI1. A clear edge is found at OC/EC=1.07, which is interpreted

234   as the OC/EC_{pri}, whereas no intercept is detected ($b \approx 0$). Following this procedure, the average

235   concentration of primary OC was 0.84 µg C m^{-3}, accounting for 35% of total OC, while average

236   OC_{sec} was 1.55 µg C m^{-3} (65%). Similar results were previously observed at a NYC Bronx site

237   (Rattigan et al., 2010).

238

239

240   **3.2 Inter-site correlations**

241   Since the Anderson-Darling test for the composite hypothesis of normality applied to

242   the data revealed that variables are generally not normally distributed at $p<0.05$, the

243   nonparametric Kruskal-Wallis ANOVA by ranks was applied to test the significance of

244   differences between the two sites. Results indicate that only SO_2, $PM_{2.5}$, and SMP in the range

245   100-200 nm concentrations were significantly different at $p<0.05$. The correlation coefficients

246   were calculated for the data over the whole sampling campaign (Table SI1) to examine the inter-

247   site relationships among pollutants. Results show that many of the variables measured at both

248   sites have moderate to strong correlations ranging from 0.60 for multiple species to 0.78 for SO_2

249   suggesting that one-third to one-half of the variance of analyzed pollutants is the same between

250   the two sites such that there were common pollutant sources contributing at both sites.

251

252   **4   DISCUSSION**

253   **4.1   Seasonal variations**

254   Seasonal variations for key species are shown in Figure 3 that depicts the monthly

255   average concentrations and the associated 75th and 99th confidence intervals calculated by

256   bootstrapping the data (n=200). Seasonal variations for all of the analyzed pollutants are

257   provided in Figure SI2. Nitrogen oxides, SO_2, NMHCs, UFPs in the first 3 size increments (20-

258   70 nm) show typical seasonal cycles with maxima in the coldest seasons (Nov-Feb) and minima

259   in the warmest months (Jun-Sept). Maxima in winter for such species are due to: (i) increase

260   emissions for building space heating; (ii) the lower mixing layer heights and possibly strong

261   thermal inversions, which limit the dispersion capacity of the atmosphere and trap the local

262   emitted pollutants close to the ground (despite the higher wind speeds in winter), and (iii) the

263   drop of ozone and hydroxyl radical and the consequent lower oxidation potential.

264   Average ozone concentrations show increased values in the warmest periods. OC and

265   sulfate show higher concentrations in the warmest periods (Jul-Aug) along with SMPs in the

266   accumulation mode (>100 nm). Increased concentrations of sulfate in warm seasons are the

267   result of the increase in concentrations of atmospheric oxidants (mainly hydroxyl radical). The

268   pattern is closely related to those of OX, air temperature and RH (Figure 3) as well as expected

269   higher summer ammonia concentrations (Paulot et al., 2014). The sulfate/SO_2 ratios describes

270   the increased speciation toward sulfate in summer: sulfate/SO_2 ratio range from values below 0.3

271   in winter to 0.8-1 from May to July.

272   The pattern of OC is strongly related to the formation of SOA, as evidenced by the

273   comparison with the estimated OC_{sec}. Alternatively, OC_{pri} is more constant through the year,

274   ranging from 0.7 to 1.1 $\mu gC\ m^{-3}$. In winter (December-February), OC_{sec} account for about 52%

275   of total OC. In summer (June-August), OC_{sec} accounts for ~69-80% of total OC. This result is

276   comparable with Yu et al. (2004) for the Northeast U.S. (77 ± 3%). These results are also

277   consistent with secondary OC accounting for 40-50% of total OC during winter and 63-73%

278   during summer at a NYC Bronx site (Rattigan et al., 2010). The pattern of OC_{sec} also well

279   matches with the seasonal variations of SOA predicted by global atmospheric chemical transport

280   models for U.S. (e.g., Liao et al., 2007). de Gouw et al. (2008) reported that organic matter in

281   NE U.S. during summer is mostly the result of formation from anthropogenic VOCs precursors

282   in urban plumes. The warmer seasons also experience increases in the emissions of biogenic

283   VOCs from plants, mostly isoprene and terpenes, which are known strong SOA precursors

284   (Carlton et al., 2009).

285   Particles in the 100-1000 nm range may originate from a variety of sources. Their

286   seasonality is very similar to sulfate and, thus, may be also the result of secondary processes.

287   This hypothesis is also partially supported by the data on the size resolved chemical composition

288   of PM in northeastern U.S. For example, Cabada et al. (2004b) and Zhang et al. (2005) reported

289   that sulfate is mostly distributed in the 100-1000 nm range at the Pittsburgh supersite.

290   Methane and CO show different behaviors. No methane data are available for May and

291   June due to equipment problems. In the U.S., up-dated emission inventories (Miller et al., 2013;

292   US EPA, 2015) report that enteric fermentation is the largest anthropogenic source of methane

293   (~26% of total emissions) followed by natural gas system and landfills. Methane showed higher

294   concentrations in April probably the result of increased release from soil and wetlands as the

295   ground warms. Carbon monoxide is primarily emitted by anthropogenic combustion (e.g.,

296   vehicular exhaust, domestic heating, industrial emissions, and biomass burning). It is also

297   formed by oxidation of methane and NMHCs (Seinfeld and Pandis, 2006). The increases in

298   winter can be primarily linked to space heating emissions and lower atmospheric dispersion

299   similar to NO_x, SO_2 and NMHCs, while the peak in April-May may result from the oxidation of

300   methane.

301   The remaining pollutants lacked significant seasonal cycles or their patterns were

302   extremely variable. $PM_{2.5}$ mass concentration showed slightly different patterns at QC and EP.

303    $PM_{2.5}$ mass concentration in QC exhibits a pattern comparable to sulfate, OC_{sec}, and particles

304   >100 nm, consistent with significant secondary processes. However, $PM_{2.5}$ lacked observable

305   seasonality at EP. This discrepancy is due to the use of different methods. Although the

306   adjustment method applied to TEOM concentrations at EP is able to approximate the data to

307 FRM, it should be noted that FRM does not capture the summer volatile PM. On the contrary,

308 the FDMS system at QC collects more of the semi-volatile material, particularly in summer.

309

310 **4.2   Weekly and daily cycles**

311   Daily cycles (Figure 4 and Figure SI3) and weekly patterns (Figure SI4) are also the

312 result of the interplay among emission strengths, photochemical processes, and micro-

313 meteorological factors. The daily cycles were computed after shifting the time to daylight saving

314 time (DST) since sources like traffic and cooking will shift by an hour at the transition from

315 standard to daylight savings and the reverse. Separating the data into two periods produces

316 better-defined diurnal profiles. Generally, most of the analyzed species (NO, NO_2, NO_x, SO_2,

317 CO, HMHCs, $PM_{2.5}$, sulfate, EC (both thermal and optical) and particles in the 20-200 nm

318 ranges) show daily peaks corresponding to the rush hours of road traffic (6–9 am) and higher

319 concentrations during weekdays. However, only some species (NO_2, SO_2, $PM_{2.5}$, and particles in

320 the 30-200 nm range) also exhibit a second typical mode related to the evening rush hours (6-11

321 pm). For these latter species, morning and evening maxima are interspersed by lower

322 concentrations that are assumed to be the result of: (i) lower emissions (less traffic); (ii) larger

323 availability of atmospheric oxidants and (iii) higher mixing layer height and wind speeds and,

324 consequently, enhanced atmospheric dispersion.

325   Ozone behaves oppositely since it depends on photochemical production during the day.

326 Ozone exhibits higher concentrations on weekends as a result of lower emissions of NO typically

327 because of lower heavy duty diesel traffic. The "weekend" effect is common in many airsheds

328 (e.g., Pires et al., 2012; Huryn and Gough, 2014). The daily and weekly variations in ozone and

329 anthropogenic emissions give rise to NO_2/NO_x ratios that show nitrogen oxide partitioning is

330 shifted significantly toward NO during the morning rush hours. Patterns in the sulfate/SO_2 ratio

331 evidence that SO_2 is always the prevailing species of sulfur. However, its transformation to

332 sulfate is enhanced by higher concentrations of ozone and oxidants.

333   Total organic carbon in $PM_{2.5}$ does not show daily cycles, but it does have a strong

334 weekly pattern with minima from Thursdays to Saturdays. Estimated primary and secondary OC

335 show peculiar cycles: OC_{pri} has patterns similar to other primary pollutants, such as NO and CO,

336 i.e. highest concentrations during weekdays and in the morning rush hours; OC_{sec} presents

337 maxima during weekends and two peaks of high concentrations during the day. The first peak is

11

338 in the afternoon correlated to the maximum solar irradiation and, thus, maximum concentrations

339 of atmospheric oxidants (OX). The second peak occurs in the evening and overnight. This could

340 indicate transport of secondary material from other locations (Strader et al., 1999) or enhanced

341 condensation of semi-volatile OC material due to lower ambient temperatures. It can also be

342 hypothesized that the oxidation of VOCs of anthropogenic and natural origins based on nitrate

343 radical oxidation can drive this behavior.

344

345 **4.3   Intra-site correlations and cross-correlations**

346   Intra-site relationships among different analyzed pollutants were investigated thought

347 the correlation coefficients. Results are provided as Figures SI5 and SI6 for QC and EP,

348 respectively. Correlation matrices were also clustered by using hierarchical cluster analysis to

349 group pollutants showing similar correlations and help the interpretation of results.

350   At QC and EP, most variable pairs show moderate to strong correlations. At QC, the

351 cluster analysis reveals that correlations may be split into 3 main groups. The first group links

352 positive correlation among particles in the smaller ranges (20-100 nm) with pollutants directly

353 emitted by combustion sources in urban environments (NO, SO_2, CO, NMHCs and EC (both

354 thermal and optical EC)), methane and NO_2. The presence of cumulative variables (NO_x and

355 THC) is not surprising since NO_2 accounts for most (68%) of NO_x and methane for most (92%)

356 of THC. The second cluster shows positive correlations among coarser SMPs (>100 nm), $PM_{2.5}$

357 mass concentration, and the main particulate species (OC and sulfate). Since sulfate is a main

358 constituent of $PM_{2.5}$ mass and OC_{sec} accounted for most of the OC mass, this cluster is likely the

359 result of the secondary aerosol contributions to the $PM_{2.5}$ mass concentrations. The presence of

360 particles >100 nm along with OC and sulfate support their assignment to being secondary

361 accumulation mode PM.

362   The last group consists only of ozone, and shows negative correlations with all other

363 pollutants. Ozone plays a key role in reacting with primary pollutants and in the generation of

364 secondary aerosol. However, ozone has weak correlations with variables in clusters 1 and 2.

365 Thus, it can be hypothesized that ozone is driven primarily by local pollutants and chemistry,

366 while sulfate and OC_{sec} PM have a non-local origin. This hypothesis will be investigated further

367 using back-trajectory models.

368   The cross-correlation functions (CCF) were computed at ±12 h lag to investigate the

369   relationships among the pollutants and between pollutants and weather parameters in more

370   detail. CCFs are calculated separately for the cold and warm seasons based on local daylight

371   saving time (EST= standard time (Nov 1 2009 – Mar 14, 2010) and EDT= Eastern daylight

372   time). The most important CCFs for QC and EP are presented in Figures SI7.

373   Generally, CCFs for pairs of variables shared by the two sites have similar profiles.

374   CCFs for pairs of species mainly emitted by primary emission sources (NO, CO, SO_2, NMHCs,

375   OC_{pri}, EC) are characterized by significant strong (>0.6) positive correlations near the 0 h lag,

376   meaning that they have concurrent daily cycles, i.e. they are potentially emitted by the same set

377   of sources and undergo to similar atmospheric processes. The correlations rapidly decrease by

378   moving lags forward and backward, indicating that the relationships among primary pollutants is

379   quite immediate.

380   The ozone-solar radiation relationship was used to investigate the photochemical

381   production of ozone. It exhibited a peak at +2 and +3 h lags, i.e. the maximal ozone

382   concentrations are delayed relative to the SR maxima. The oxidative chain driven by ozone were

383   further analyzed in terms of the NO_2–O_3 and NO_2–NO pairs. Strong correlations (negative and

384   positive, respectively) occur at lag 0 and reflect the fast kinetics of NO oxidation by ozone and

385   hydroxyl radical (Finlayson Pitts and Pitts, 2000). The CCFs for the methane-ozone and sulfate-

386   ozone pairs show weak correlations (0.3<r<0.6) over all lag values. Although the correlations are

387   weak, the CCF for sulfate-ozone has positive values during the warm season and negative in cold

388   periods reflecting the temperature dependence of the kinetics of S(IV) oxidation. It can be also

389   hypothesized that negative CCF of sulfate-ozone in winter are due to the local sulfate production

390   in NYC driven by the use of high sulfur-content home heating oils, whereas there is limited O_3

391   production.

392   CCFs for sulfate-$PM_{2.5}$ and OC_{sec}-$PM_{2.5}$ present moderate to strong (0.4-0.6)

393   correlations over all lags. This result shows that sulfate and OC_{sec} drive the $PM_{2.5}$ mass

394   concentrations, and also indicates that secondary particle formation requires more than 12 h, i.e.

395   such processes do not occur locally.

396   CCFs among SMPs and pollutants shared by the two sites are provided in Figures SI8

397   and SI9. Particles generally show significant positive correlations with NO, NO_2, SO_2 and $PM_{2.5}$

398   at lag 0. However, correlations with NO, NO_2 and SO_2 are higher for particles in the 50-100 nm

399   range, while correlations with $PM_{2.5}$ increase by increasing the particle size. This latter result is

400   largely expected, since large particles mostly contribute to the $PM_{2.5}$ mass.

401

402   **4.4   Identification of local sources**

403   CBPF plots are used to identify the potential local emission sources. The hourly air

404   pollutant concentrations were matched with wind speed and direction values from the two

405   weather stations. The criterion value was set at >75th percentile. All data were used, e.g., no

406   wind calm hours were removed. The results are provided in Figure 5 for QC and Figure SI10 for

407   EP. For data collected at QC, CBPF were calculated separately for the cold and warm seasons

408   split based on the seasonal time change (Figures SI11 and SI12).

409   Generally, CBPFs at QC and EP show similar profiles for most of the analyzed species.

410   Such profiles remain constant through the cold and warm seasons. However, higher probabilities

411   of concentrations >75th percentile are found during the cold season for all of the locally emitted

412   pollutants. In addition, there is less conversion of primary pollutants during winter due to

413   reduced photochemical processes. High probabilities of NO, NO_2, CO, NMHCs, OC_{pri}, EC and

414   SMP in the 30-100 nm range were attained during calm wind periods or under low/moderate

415   wind speed (<5 m s^{-1}) with no prevailing direction. This pattern is compatible with the dilution

416   effect driven by winds and the consequent advection of fresh air masses, and is also explained by

417   the inverse relationships of the daily cycles between wind speed and primary pollutants (Figure

418   4). The highest wind speeds were observed in the afternoon and were concurrent with minimal

419   concentrations of the local-emitted species. These results further support attribution of NO, NO_2,

420   CO, NMHCs, OC_{pri}, EC and SMP in the 30-100 nm range to local emissions and/or fast

421   atmospheric processes.

422   SO_2 shows increased probabilities with moderate westerly winds, i.e. toward the lower

423   end of Manhattan. This direction is likely the result of emissions from central heating systems of

424   the large buildings   In NYC, the primary fuels used for space and water heating are fuel oils and

425   natural gas. A large number of small residential and commercial buildings use distillate oil No. 2,

426   while many larger buildings burn the less refined No. 6 (residual oil) with higher emission

427   factors (US EPA, 2010; Kheirbek et al., 2014) or a mixture of Nos. 2 and 6 to produce No. 4 oil.

428   In 2009-2010, No. 2 oil contained 0.2% sulfur (by weight), while the content in Nos. 4 and 6 was

429   higher (0.3%). The annual building energy consumption by block area in NYC in 2009 reported

430   by Howard et al., 2012 shows that Manhattan has very high energy consumptions with respect to

431   other boroughs and it is therefore likely to emit higher amounts of SO_2. However, shipping is

432   another known strong source of SO_2 (e.g., Isakson et al., 2001; Eyring et al., 2005) and the CBPF

433   is compatible with emissions from the container port at the Port of Elizabeth, NJ.

434   Methane, $PM_{2.5}$, sulfate, OC_{sec} and particles >100 nm exhibit high probabilities for

435   moderate (4-7 m s^{-1}) winds blowing from SW. The highest probabilities are attained for air

436   masses from Brooklyn. However, the relative high wind speeds associated with the CBPF

437   indicate that the advection of air masses over Manhattan has the potential for raising their

438   concentrations. Despite sulfate and OC_{sec} are related to secondary processes and, thus, may have

439   a probable regional origin, it can be hypothesized that domestic heating and traffic may also

440   contribute to their concentrations on a local scale. Ozone show increased probabilities for strong

441   (>5 m s^{-1}) winds blowing from SSE. Thus, high ozone concentrations are observed when the

442   winds blow from directions not heavily impacted by traffic, i.e. when NO is not sufficient to

443   titrate out the O_3.

444   CBPF for the smallest particles (20-30 nm) show a different pattern. At QC, the higher

445   concentrations are for winds blowing from NW, while the probability for calm wind periods is

446   very low (<0.3). On the contrary, CBPF at EP shows a profile similar to other primary pollutants

447   (moderate winds from W). The pattern at QC is not found for any other species and indicates a

448   source of ultrafine particles in the nucleation mode toward NW. Potential emissions from high

449   density of urban areas and the presence of main roads (e.g., Long Island Expressway, Van Wyck

450   and Whitestone Expressways, Grand Central Parkway) are compatible with this result. High-

451   density urban areas and frequently congested main roads are widespread in Queens. For

452   example, the Long Island Expressway generally experiences the highest traffic volumes in

453   Queens County, in excess of 200,000 vehicles day^{-1} and it is frequently congested. As a

454   consequence, minor roads in the area are also frequently congested. In addition, a large number

455   of school buses moves in the area due to the College and other schools.

456   In addition to road traffic as a major source, the nucleation mode particles may be

457   attributable to the emissions from LaGuardia Airport, approximately 5 km NW of QC. Aircraft

458   emit ultrafine particles in the nucleation range (Masiol and Harrison, 2014; Lobo et al., 2015),

459   thus airports are known sources of UFPs. For example, Hudda et al. (2014) reported that

460   emissions from the Los Angeles International Airport increase PNC 4-fold at 10 km downwind,

461 while Keuken et al. (2015) reported that the particle number size distributions downwind of

462 Schiphol Airport (The Netherlands) was dominated by ultrafine (10 to 20 nm) particles.

463 LaGuardia Airport is one of three commercial airports for NYC and had ~379,000 plane

464 movements in 2010.

465

466 **4.5   Potential distant sources**

467   The potential locations of distant sources were evaluated through PSCF analyses. The

468 hourly air pollutant concentrations were matched with the back trajectories. The criterion value

469 was set to concentrations >75th percentile. The PSCF surfaces were smoothed to decrease the

470 noise due to the uncertainties of trajectories and to enhance the interpretability of maps. Results

471 are shown in Figure 6 for QC and Figure SI13 for EP. For QC, the PSCF values were calculated

472 separately for the cold and warm seasons (Figures SI14 and SI15).

473   Results show that continental eastern U.S. particularly the upper Ohio River Valley

474 region was the highest probability source area for almost all the pollutants having likely regional

475 origins, including SO_2, CH_4, $PM_{2.5}$, sulfate, OC_{sec}, and particles >50 nm. These patterns are

476 almost constant during the cold and warm seasons. The probabilities for NO_2, SO_2, CO, NMHCs,

477 OC_{pri}, EC and particles in the 50-100 nm range are generally less than 0.5. The maps do show

478 probabilities >0.5 for methane, $PM_{2.5}$, sulfate and particles >100 nm. The maps for both sites

479 clearly show that the potential effects of regional transports rise with increasing particle

480 dimensions, with the highest probabilities for particles in the >200 nm range.

481   PSCF maps for particles >50 nm corresponded with the modeled emissions from the

482 major UFP sources in the Eastern U.S. during summer as reported by Posner and Pandis (2015).

483 The PSCF maps for particles in the 20-50 range do not show any pattern. The lack of any

484 significant PSCF probability for finest particles means that they originate primarily from local

485 sources and are not transported over long distances.

486

487 **5.   CONCLUSIONS**

488 This study has provided direct information on the concentrations and trends of key air pollutants

489 over high densely urbanized areas of NYC and Long Island. Primary and secondary OC are also

490 estimated. Results enable some general considerations that can be summarized as follows:

491 • The seasonal, weekly and diurnal cycles of pollutants primarily emitted by anthropogenic
492   sources (NO, SO$_2$, CO, NMHCs, OC$_{pri}$, EC and 30-100 nm particles) are strongly shaped by
493   emission factors, human habits, photochemical processes and weather. Typical sinusoidal
494   seasonality with maxima during cold seasons and uni/bimodal daily cycles related to rush
495   hours are found for most pollutants. Nitrogen dioxide also follows this behavior due to the
496   fast oxidation of NO. Intra-species analysis by means of cross-correlations has also pointed
497   out the strong relationships among primary air pollutants by showing high positive
498   correlations at 0 h lag. Primary pollutants increase during wind calm periods or under slow
499   wind regimes and the CBPF analysis has evidenced that they are emitted locally. In addition,
500   no significant effects of regional transports of primary species are evidenced from PSCF
501   analysis. Results indicate different potential local sources: road traffic is the most probable
502   source of nitrogen oxides, CO, NMHCs, OC$_{pri}$, EC and 30-100 nm particles, while domestic
503   heating burning fuel oils and shipping for SO$_2$.
504 • PM$_{2.5}$ and coarser particles are strongly related to secondary processes, as evidenced by the
505   comparison with sulfate and estimated OC$_{sec}$. They show comparable seasonal and diurnal
506   profiles, high correlations and relatively high lagged correlations over long periods (+/- 12
507   h). Also, CBPF results show that the advection of regional air masses has a potential effect in
508   raising their concentrations, while PSCF pointed out the Eastern continental U.S. as most
509   probable remote source area.
510 • Both local and regional sources can be found for UFPs in the nucleation range (<30 nm).
511   Results indicate that LaGuardia airport is a potential local source at Queens, while PSCF
512   analysis does not reveal any dominant remote source area.
513 • Ozone is linked to the photochemical production and is delayed (+2 h) with respect the
514   maxima solar radiation. Correlations and diurnal cycles point out on its potential high effect
515   as oxidant for primary species. Despite the large set of ozone-precursor emitted by
516   anthropogenic sources within NYC boundaries, CBPF analysis has revealed that most O$_3$ is
517   advected during high wind regimes, but not dominant source areas are evidenced by PSCF.
518
519
520
521

530

531 **REFERENCES**

532 Adam, M., Schikowski, T., Carsin, A. E., Cai, Y., Jacquemin, B., Sanchez, M., et al., 2015.
533   Adult lung function and long-term air pollution exposure. ESCAPE: a multicentre cohort
534   study and meta-analysis. European Respiratory Journal, 45(1), 38-50.
535 Anderson, J. O., Thundiyil, J. G., Stolbach, A., 2012. Clearing the air: a review of the effects of
536   particulate matter air pollution on human health. Journal of Medical Toxicology 8(2),
537   166-175.
538 Ashbaugh, L.L., Malm, W.C., Sadeh, W.Z., 1985. A residence time probability analysis of sulfur
539   concentrations at ground Canyon National Park. Atmospheric Environment 19 (8), 1263-
540   1270.
541 Barnes, I., Hjorth, J. Mihalopoulos, N., 2006. Dimethyl sulfide and dimethyl sulfoxide and their
542   oxidation in the atmosphere. Chemical Reviews 106(3), 940-975.
543 Bauer, J.J., Yu, X.Y., Cary, R., Laulainen, N. and Berkowitz, C., 2009. Characterization of the
544   sunset semi-continuous carbon aerosol analyzer. Journal of the Air & Waste Management
545   Association 59(7), pp.826-833.
546 Benson, D.R., Yu, J.H., Markovich, A., Lee, S.-H., 2011. Ternary homogeneous nucleation of
547   H2SO4, NH3, and H2O under conditions relevant to the lower troposphere. Atmospheric
548   Chemistry and Physics 11, 4755-4766.
549 Brown, S. S., deGouw, J. A., Warneke, C., Ryerson, T. B., Dubé, W. P., Atlas, E., Weber, R. J.,
550   Peltier, R. E., Neuman, J. A., Roberts, J. M., Swanson, A., Flocke, F., McKeen, S. A.,
551   Brioude, J., Sommariva, R., Trainer, M., Fehsenfeld, F. C., Ravishankara, A. R.., 2009.
552   Nocturnal isoprene oxidation over the Northeast United States in summer and its impact
553   on reactive nitrogen partitioning and secondary organic aerosol. Atmospheric Chemistry
554   and Physics 9, 3027-3042.
555 Buckley, S.M., Mitchell, M.J., 2011. Improvements in urban air quality: case studies from New York
556   State, USA. Water, Air & Soil Pollution 214, 93-106.
557 Cabada J.C., Pandis S.N., Subramanian R., Robinson A.L., Polidori A., Turpin B., 2004a.
558   Estimating the secondary organic aerosol contribution to PM2.5 using the EC tracer
559   method. Aerosol Science & Technology 38(S1), 140-155.
560 Cabada, J.C., Rees, S., Takahama, S., Khlystov, A., Pandis, S.N., Davidson, C.I. Robinson, A.L.,
561   2004b. Mass size distributions and size resolved chemical composition of fine particulate
562   matter at the Pittsburgh supersite. Atmospheric Environment 38(20), 3127-3141

563   Carlton, A.G., Wiedinmyer, C., Kroll, J.H., 2009. A review of Secondary Organic Aerosol
564   (SOA) formation from isoprene. Atmospheric Chemistry and Physics, 9(14), 4987-5005.
565   Carslaw, D.C. K. Ropkins, 2012. openair — an R package for air quality data analysis.
566   Environmental Modelling & Software 27–28, 52–61.
567   Carslaw, D.C., Beevers, S.D., Ropkins, K., Bell, M.C., 2006. Detecting and quantifying aircraft
568   and other on-airport contributions to ambient nitrogen oxides in the vicinity of a large
569   international airport. Atmospheric Environment 40, 5424–5434.
570   Colette, A., Granier, C., Hodnebrog, Ø., Jakobs, H., Maurizi, A., Nyiri, A., Bessagnet, B.,
571   D'Angiola, A., D'Isidoro, M., Gauss, M., Meleux, F., Memmesheimer, M., Mieville, A.,
572   Rouïl, L., Russo, F., Solberg, S., Stordal, F., Tampieri, F., 2011. Air quality trends in
573   Europe over the past decade: a first multi-model assessment. Atmospheric Chemistry and
574   Physics 11(22), 11657-11678.
575   Day, M.C., Zhang, M. Pandis, S.N., 2015. Evaluation of the ability of the EC tracer method to
576   estimate secondary organic carbon. Atmospheric Environment 112, 317-325.
577   de Gouw, J.A., Brock, C.A., Atlas, E.L., Bates, T.S., Fehsenfeld, F.C., Goldan, P.D., Holloway,
578   J.S., Kuster, W.C., Lerner, B.M., Matthew, B.M. Middlebrook, A.M., 2008. Sources of
579   particulate matter in the northeastern United States in summer: 1. Direct emissions and
580   secondary formation of organic matter in urban plumes. Journal of Geophysical
581   Research: Atmospheres 113(D8).
582   Donahue, N.M., Robinson, A.L. Pandis, S.N., 2009. Atmospheric organic particulate matter:
583   From smoke to secondary organic aerosol. Atmospheric Environment 43(1), pp.94-106.
584   Duncan, B.N., Lamsal, L.N., Thompson, A.M., Yoshida, Y., Lu, Z., Streets, D.G., Hurwitz,
585   M.M. Pickering, K.E., 2016. A space-based, high-resolution view of notable changes in
586   urban NO_x pollution around the world (2005–2014). Journal of Geophysical Research:
587   Atmospheres 121, doi:10.1002/2015JD024121.
588   Eyring, V., Köhler, H.W., Van Aardenne, J. Lauer, A., 2005. Emissions from international
589   shipping: 1. The last 50 years. Journal of Geophysical Research: Atmospheres 110(D17).
590   Felton D., 2005. Modifying 50 ºC TEOM Data to be more "FRM like" for AQI Reporting using
591   a Non-linear Correction based on the Julian Day. 2005 AAAR Meeting, February 7-11,
592   2005, Atlanta, GA, USA.
593   Finlayson-Pitts, B.J., Pitts, J.N., 2000. Chemistry of the Upper and Lower Atmosphere: Theory,
594   Experiments, and Applications. Academic Press, San Diego, p. 969.
595   Franklin, B. A., Brook, R., Pope, C. A., 2015. Air Pollution and Cardiovascular Disease. Current
596   problems in Cardiology, 40(5), 207-238.
597   Götschi, T., Heinrich, J., Sunyer, J., Künzli, N., 2008. Long-term effects of ambient air pollution
598   on lung function: a review. Epidemiology 19(5), 690-701.
599   Hand, J. L., Schichtel, B. A., Malm, W. C., Pitchford, M. L., 2012a. Particulate sulfate ion
600   concentration and SO 2 emission trends in the United States from the early 1990s through
601   2010. Atmospheric Chemistry and Physics 12(21), 10353-10365.
602   Hand, J.L., Schichtel, B.A., Pitchford, M., Malm, W.C. Frank, N.H., 2012b. Seasonal
603   composition of remote and urban fine particulate matter in the United States. Journal of
604   Geophysical Research 117(D5).
605   Henze, D.K., Seinfeld, J.H., Ng, N.L., Kroll, J.H., Fu, T.M., Jacob, D.J. and Heald, C.L., 2008.
606   Global modeling of secondary organic aerosol formation from aromatic hydrocarbons:
607   high-vs. low-yield pathways. Atmospheric Chemistry and Physics 8(9),2405-2420.

608 Holmes, N.S., 2007. A review of particle formation events and growth in the atmosphere in the
609   various environments and discussion of mechanistic implications. Atmospheric
610   Environment 41, 2183-2201.
611 Hopke, P.K., 2016. Review of receptor modeling methods for source apportionment. Journal of
612   the Air & Waste Management Association, doi:10.1080/10962247.2016.1140693.
613 Howard, B., Parshall, L., Thompson, J., Hammer, S., Dickinson, J. Modi, V., 2012. Spatial
614   distribution of urban building energy consumption by end use. Energy and Buildings 45,
615   141-151.
616 Hudda, N, Gould, T., Hartin, K., Larson, T.V., Fruin, S.A., 2014. Emissions from an
617   international airport increase particle number concentrations 4-fold at 10 km downwind.
618   Environmental Science & Technology 48, 6628−6635.
619 Huryn, S.M., Gough, W.A., 2014. Impact of urbanization on the ozone weekday/weekend effect
620   in Southern Ontario, Canada, Urban Climate 8, 11-20.
621 Isakson, J., Persson, T.A. Lindgren, E.S., 2001. Identification and assessment of ship emissions
622   and their effects in the harbour of Göteborg, Sweden. Atmospheric Environment 35(21),
623   3659-3666.
624 Jenkin, M.E. and Hayman, G.D., 2000. Photochemical ozone creation potentials for oxygenated
625   volatile organic compounds: sensitivity to variations in kinetic and mechanistic
626   parameters. Atmospheric Environment 33(8), 1275-1293.
627 Kara, M., Hopke, P.K., Dumanoglu, Y., Altiok, H., Elbir, T., Odabasi, M., Bayram, A., 2015.
628   Characterization of PM Using Multiple Site Data in a Heavily Industrialized Region of
629   Turkey. Aerosol and Air Quality Research 15, 11–27.
630 Keuken, M.P., Moerman, M., Zandveld, P., Henzing, J.S., Hoek, G., 2015. Total and size-
631   resolved particle number and black carbon concentrations in urban areas near Schiphol
632   airport (the Netherlands). Atmospheric Environment 104 132-142.
633 Kheirbek, I., Haney, J., Douglas, S., Ito, K., Caputo Jr, S. Matte, T., 2014. The public health
634   benefits of reducing fine particulate matter through conversion to cleaner heating fuels in
635   New York City. Environmental Science & Technology 48(23), 13573-13582.
636 Kim, E., Hopke, P.K., Edgerton, E.S., 2003. Source identification of Atlanta aerosol by positive
637   matrix factorization, Journal of the Air & Waste Management Association 53, 731-739.
638 Kley, D., Kleinmann, M., Sanderman, H., Krupa, S., 1999. Photochemical oxidants: state of the
639   science. Environmental Pollution 100, 19-42.
640 Knibbs, L.D., Cole-Hunter, T. Morawska, L., 2011. A review of commuter exposure to ultrafine
641   particles and its health effects. Atmospheric Environment 45(16), 2611-2622.
642 Kroll, J.H. and Seinfeld, J.H., 2008. Chemistry of secondary organic aerosol: Formation and
643   evolution of low-volatility organics in the atmosphere. Atmospheric Environment 42(16),
644   3593-3624.
645 Lane T.N., Pandis S.N., 2007. Predicted Secondary Organic Aerosol Concentrations from the
646   Oxidation of Isoprene in the Eastern United States. Environmental Science and
647   Technology 41 (11), pp 3984–3990
648 Lanzinger, S., Schneider, A., Breitner, S., Stafoggia, M., Erzen, I., Dostal, M., Pastorkova, A.,
649   Bastian, S., Cyrys, J., Zscheppang, A. Kolodnitska, T., 2016. Associations between
650   ultrafine and fine particles and mortality in five central European cities—Results from the
651   UFIREG study. Environment International 88, 44-52.

652 Laumbach, R. J., Kipen, H. M., 2012. Respiratory health effects of air pollution: update on
653   biomass smoke and traffic pollution. Journal of Allergy and Clinical Immunology 129(1),
654   3-11.
655 Lee, J.H., Hopke, P.K., 2006. Apportioning sources of PM2.5 in St. Louis, MO using speciation
656   trends network data. Atmospheric Environment 40, 360-377.
657 Liao, H., Henze, D.K., Seinfeld, J.H., Wu, S. and Mickley, L.J., 2007. Biogenic secondary
658   organic aerosol over the United States: Comparison of climatological simulations with
659   observations. Journal of Geophysical Research: Atmospheres 112(D6).
660 Lim, H.J., Turpin, B.J., 2002. Origins of primary and secondary organic aerosol in Atlanta:
661   results of time-resolved measurements during the Atlanta supersite experiment.
662   Environmental Science and Technology 36, 4489-4496.
663 Lobo, P., Hagen, D. E., Whitefield, P. D., Raper, D., 2015. PM emissions measurements of in-
664   service commercial aircraft engines during the Delta-Atlanta Hartsfield Study.
665   Atmospheric Environment 104, 237-245.
666 Loomis, D., Grosse, Y., Lauby-Secretan, B., Ghissassi, F. E., Bouvard, V., Benbrahim-Tallaa, L.
667   Guha, N., Baan, R., Mattock, H., Straif, K., 2013. The carcinogenicity of outdoor air
668   pollution. The Lancet Oncology, 14(13), 1262-1263.
669 Masiol, M., Harrison, R.M., 2014. Aircraft engine exhaust emissions and other airport-related
670   contributions to ambient air pollution: A review. Atmospheric Environment 95, 409-455.
671 Medved, A., Dorman, F., Kaufman, S.L., and Pöcher, A., 2000. A New Corona-based Charger
672   for Aerosol Particles. Journal of Aerosol Science 31, 616-617.
673 Miller, S.M., Wofsy, S.C., Michalak, A.M., Kort, E.A., Andrews, A.E., Biraud, S.C.,
674   Dlugokencky, E.J., Eluszkiewicz, J., Fischer, M.L., Janssens-Maenhout, G. Miller, B.R.,
675   2013. Anthropogenic emissions of methane in the United States. Proceedings of the
676   National Academy of Sciences, 110(50), 20018-20022.
677 Ng, N.L., Kroll, J.H., Chan, A.W.H., Chhabra, P.S., Flagan, R.C. Seinfeld, J.H., 2007. Secondary
678   organic aerosol formation from m-xylene, toluene, and benzene. Atmospheric Chemistry
679   and Physics, 7(14),3909-3922.
680 NY State Dep. Environmental Conservation, 2016. 2014 Region 2 Air Quality Data. Available
681   at: http://www.dec.ny.gov/chemical/29310.html [last accessed: Jan 2016]
682 NYC Department of Health and Mental Hygiene, 2013a. New York City Trends in Air Pollution
683   and its Health Consequences. New York City Department of Health and Mental Hygiene,
684   New York, NY.
685 NYC Department of Health and Mental Hygiene, 2013b. Air Pollution and the Health of New
686   Yorkers: The Impact of Fine Particles and Ozone. New York City Department of Health
687   and Mental Hygiene, New York, NY.
688 NREL (National Renewable Energy Laboratory), 2012. National Solar Radiation Datadase 1991-
689   2010 Update: User's manual. NREL Technical report NREL/TP-5500-54824.
690 Ostro, B., Hu, J., Goldberg, D., Reynolds, P., Hertz, A., Bernstein, L. Kleeman, M.J., 2015.
691   Associations of Mortality with Long-Term Exposures to Fine and Ultrafine Particles,
692   Species and Sources: Results from the California Teachers Study Cohort. Environmental
693   Health Perspectives 123(6), 549-556.
694 Parrish D.D., Singh H.B., Molina L., Madronich S., 2011. Air quality progress in North
695   American megacities: A review. Atmospheric Environment 45(39), 7015-7025.
696 Paulot, F., Jacob, D.J., Pinder, R.W., Bash, J.O., Travis, K. and Henze, D.K., 2014. Ammonia
697   emissions in the United States, European Union, and China derived by high-resolution

698   inversion of ammonium wet deposition data: Interpretation with a new agricultural
699   emissions inventory (MASAGE_NH3). Journal of Geophysical Research: Atmospheres
700   119(7), pp.4343-4364.
701 Pekney, N. J., Davidson, C. I., Zhou, L., Hopke, P. K., 2006. Application of PSCF and CPF to
702   PMF-Modeled Sources of PM2.5 in Pittsburgh. Aerosol Science & Technology 40(10),
703   952-961.
704 Pires, J. C. M. (2012), Ozone Weekend Effect Analysis in Three European Urban Areas. Clean
705   Soil Air Water, 40: 790–797. doi: 10.1002/clen.201100410
706 Polidori, A., Turpin, B.J., Davidson, C.I., Rodenburg, L.A. Maimone, F., 2008. Organic PM2.5:
707   Fractionation by polarity, FTIR spectroscopy, and OM/OC ratio for the Pittsburgh
708   aerosol. Aerosol Science and Technology, 42(3), 233-246.
709 Polissar, A. V., P. K. Hopke, and J. M. Harris. 2001. Source Regions for Atmospheric Aerosol
710   Measured at Barrow, Alaska. Environmental Science and Technology 35 (21): 4214–26.
711 Pope, C., Burnett, R. T., Turner, M. C., Cohen, A., Krewski, D., Jerrett, M., Gapstur, S.M.,
712   Thun, M. J., 2011. Lung cancer and cardiovascular disease mortality associated with
713   ambient air pollution and cigarette smoke: shape of the exposure-response relationships.
714   Environmental Health Perspectives 119(11), 1616-21.
715 Posner, L.N., Pandis, S.N., 2015. Sources of ultrafine particles in the Eastern United States.
716   Atmospheric Environment 111, 103–112.
717 Rattigan, O.V., Felton H.D., Bae M.S., Schwab J.J. , Demerjian K.L., 2010. Multi-year hourly
718   PM2.5 carbon measurements in New York: Diurnal, day of week and seasonal patterns.
719   Atmospheric Environment 44, 2043-2053.
720 Rattigan, O.V., Civerolo K.L., Felton H.D., Schwab J.J., Demerjian K.L., 2016. Long Term
721   Trends in New York: PM2.5 mass and Particle Components, doi:
722   10.4209/aaqr.2015.05.0319.
723 R Development Core Team, 2008. R: A language and environment for statistical computing. R
724   Foundation for Statistical Computing, Vienna, Austria. ISBN 3-900051-07-0.
725 Rolph, G.D., 2016. Real-time Environmental Applications and Display sYstem (READY)
726   Website (http://www.ready.noaa.gov). NOAA Air Resources Laboratory, College Park,
727   MD.
728 Seinfeld, J.H., Pandis, S.N., 2006. Atmospheric Chemistry and Physics: From Air Pollution to
729   Climate Change, second ed. John Wiley & Sons, NewYork.
730 Shah, A. S., Langrish, J. P., Nair, H., McAllister, D. A., Hunter, A. L., Donaldson, K., Newby,
731   D.E., Mills, N. L. 2013. Global association of air pollution and heart failure: a systematic
732   review and meta-analysis. The Lancet 382(9897), 1039-1048.
733 Smith, S.J., Aardenne, J.V., Klimont, Z., Andres, R.J., Volke, A., Delgado Arias, S., 2011.
734   Anthropogenic sulfur dioxide emissions: 1850-2005. Atmospheric Chemistry and Physics
735   11, 1101-1116.
736 Stein, A.F., Draxler, R.R, Rolph, G.D., Stunder, B.J.B., Cohen, M.D., and Ngan, F., 2015.
737   NOAA's HYSPLIT atmospheric transport and dispersion modeling system. Bulletin of
738   the American Meteorological Society 96, 2059-2077.
739 Stockwell, W.R., 1994. The effect of gas-phase chemistry on aqueous-phase sulfur dioxide
740   oxidation rates. Journal of Atmospheric Chemistry 19, 317-329.
741 Stockwell, W.R., Calvert, J.G., 1983. The mechanism of the HO-SO2 reaction. Atmospheric
742   Environment 17, 2231-2235.

743 Stohl, A., 1998. Computation, accuracy and applications of trajectories- review and
744   bibliography. Atmospheric Environment 32, 947-966.
745 Strader, R., Lurmann, F., Pandis, S.N., 1999. Evaluation of secondary organic aerosol formation
746   in winter. Atmospheric Environment 33, 48494863.
747 Strak, M.M., Janssen, N.A., Godri, K.J., Gosens, I., Mudway, I.S., Cassee, F.R., Lebret, E.,
748   Kelly, F.J., Harrison, R.M., Brunekreef, B. and Steenhof, M., 2012. Respiratory health
749   effects of airborne particulate matter: the role of particle size, composition, and oxidative
750   potential-the RAPTES project. Environmental Health Perspectives, 120(8), pp.1183-
751   1189.
752 Straif, K., Cohen, A. Samet, J., 2013. Air pollution and cancer. IARC scientific publication, 161,
753   International Agency for Research on Cancer, 150 cours Albert Thomas, 69372 Lyon
754   Cedex 08, France, 2013. Available from
755   http://www.iarc.fr/en/publications/books/sp161/AirPollutionandCancer161.pdf.
756 Turner, M. C., Krewski, D., Pope III, C. A., Chen, Y., Gapstur, S. M., Thun, M. J., 2011. Long-
757   term ambient fine particulate matter air pollution and lung cancer in a large cohort of
758   never-smokers. American Journal of Respiratory and Critical Care Medicine, 184(12),
759   1374-1381.
760 Turpin, B.J., Huntzicker, J.J., 1995. Identification of secondary organic aerosol episodes and
761   quantification of primary and secondary organic aerosol concentrations during SCAQS.
762   Atmospheric Environment 29 (23), 3527-3544.
763 Uria-Tellaetxe, I., Carslaw, D.C., 2014. Conditional bivariate probability function for source
764   identification. Environmental Modelling & Software 59 (59), 1–9.
765 US EPA, 2010. AP-42, 5th ed., Chapter 1: Regional Combustion Sources; U.S. Environmental
766   Protection Agency, 2010; Vol. 1. Available at:
767   http://www3.epa.gov/ttnchie1/ap42/ch01/final/c01s03.pdf [last accessed on February
768   2016]
769 US EPA, 2015. Inventory of U.S. Greenhouse Gas Emissions and Sinks: 1990 – 2013. US EPA
770   document 430-R-15-004. US EPA, Washington DC, USA. Available at:
771   http://www3.epa.gov/climatechange/Downloads/ghgemissions/US-GHG-Inventory-2015-
772   Main-Text.pdf [last accessed on January 2016]
773 Watson, J.G., Chow, J.C., Fujita, E.M., 2001. Review of volatile organic compounds source
774   apportionment by chemical mass balance. Atmospheric Environment 35, 1567–1584.
775 Yu, S., Dennis, R.L., Bhave, P.V. Eder, B.K., 2004. Primary and secondary organic aerosols
776   over the United States: estimates on the basis of observed organic carbon (OC) and
777   elemental carbon (EC), and air quality modeled primary OC/EC ratios. Atmospheric
778   Environment 38(31),5257-5268.
779 Yu, S., Bhave, P.V., Dennis, R.L. Mathur, R., 2007. Seasonal and regional variations of primary
780   and secondary organic aerosols over the continental United States: Semi-empirical
781   estimates and model evaluation. Environmental Science & Technology, 41(13), pp.4690-
782   4697.
783 Zhang, Q., Canagaratna, M.R., Jayne, J.T., Worsnop, D.R. Jimenez, J.L., 2005. Time-and
784   size-resolved chemical composition of submicron particles in Pittsburgh: Implications for
785   aerosol sources and processes. Journal of Geophysical Research: Atmospheres, 110(D7)
786 Zhang, R., Khalizov, A., Wang, L., Hu, M., Xu, W., 2011. Nucleation and growth of
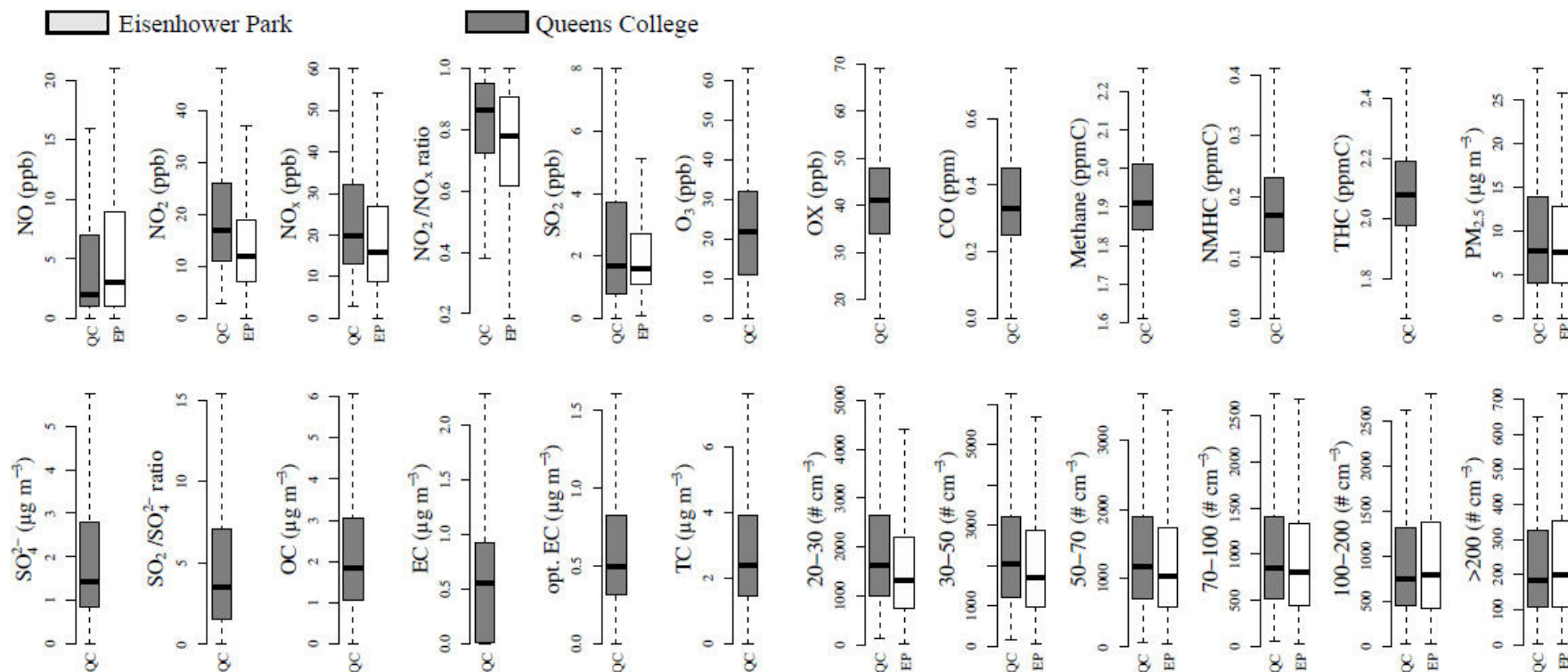787   nanoparticles in the atmosphere. Chemical Reviews 112, 1957-2011.
788

Figure 1. Map of the study area showing the two sampling sites (QC= Queens College; EP= Eisenhower Park) and wind roses for the sampling period (July 2009-July 2010) at the two weather stations (LGA= LaGuardia Airport; FRG= Republic Airport).

Figure 2. Boxplots of the analyzed pollutants. Lines= medians, boxes= 25th-75th percentile ranges, whiskers= ±1.5*inter-quartile ranges.
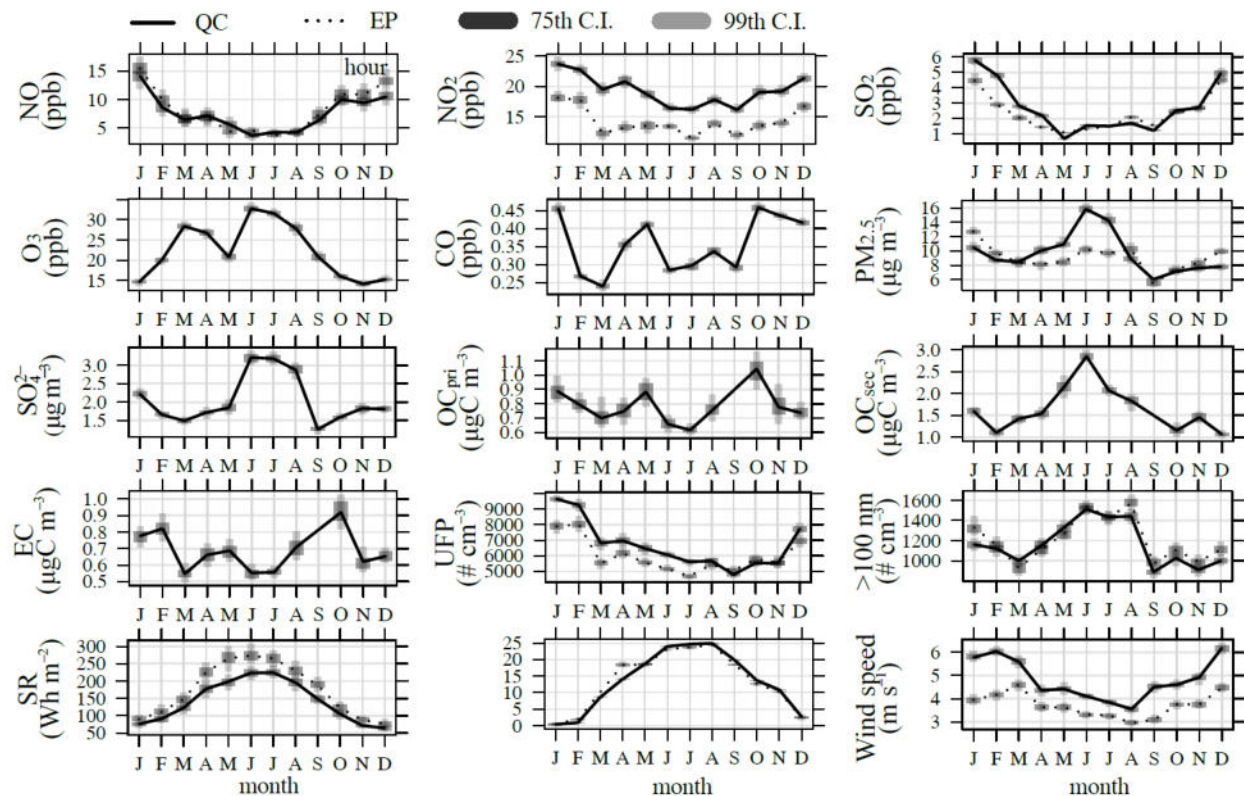
Figure 3. Seasonal variations of all monitored pollutants, derived parameters and some weather parameters. Each plot reports the monthly average concentrations as a filled line and the associated 75th and 99th confidence intervals calculated by bootstrapping the data (n=200).
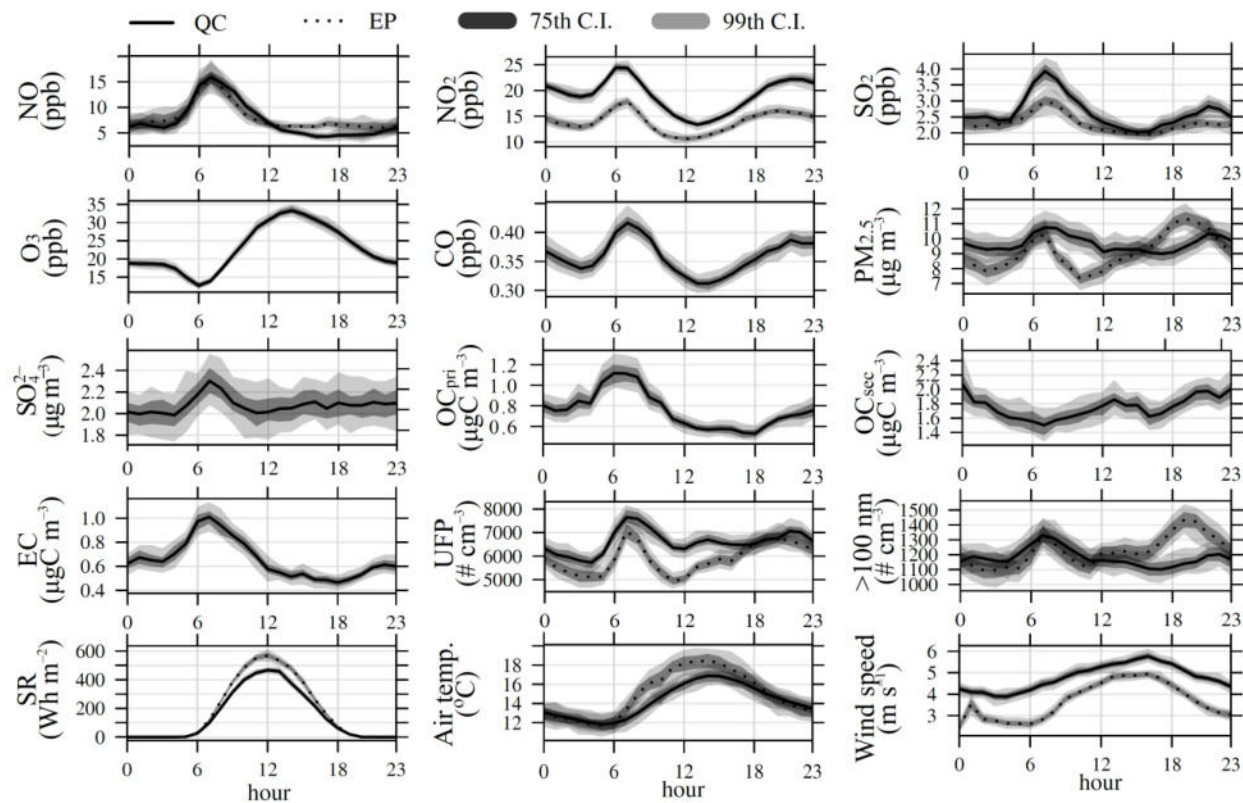
Figure 4. Diurnal variations in concentrations of measured pollutants. Each plot reports the average concentration as a filled line and the associated 75th and 99th confidence intervals calculated by bootstrapping the data (n=200).
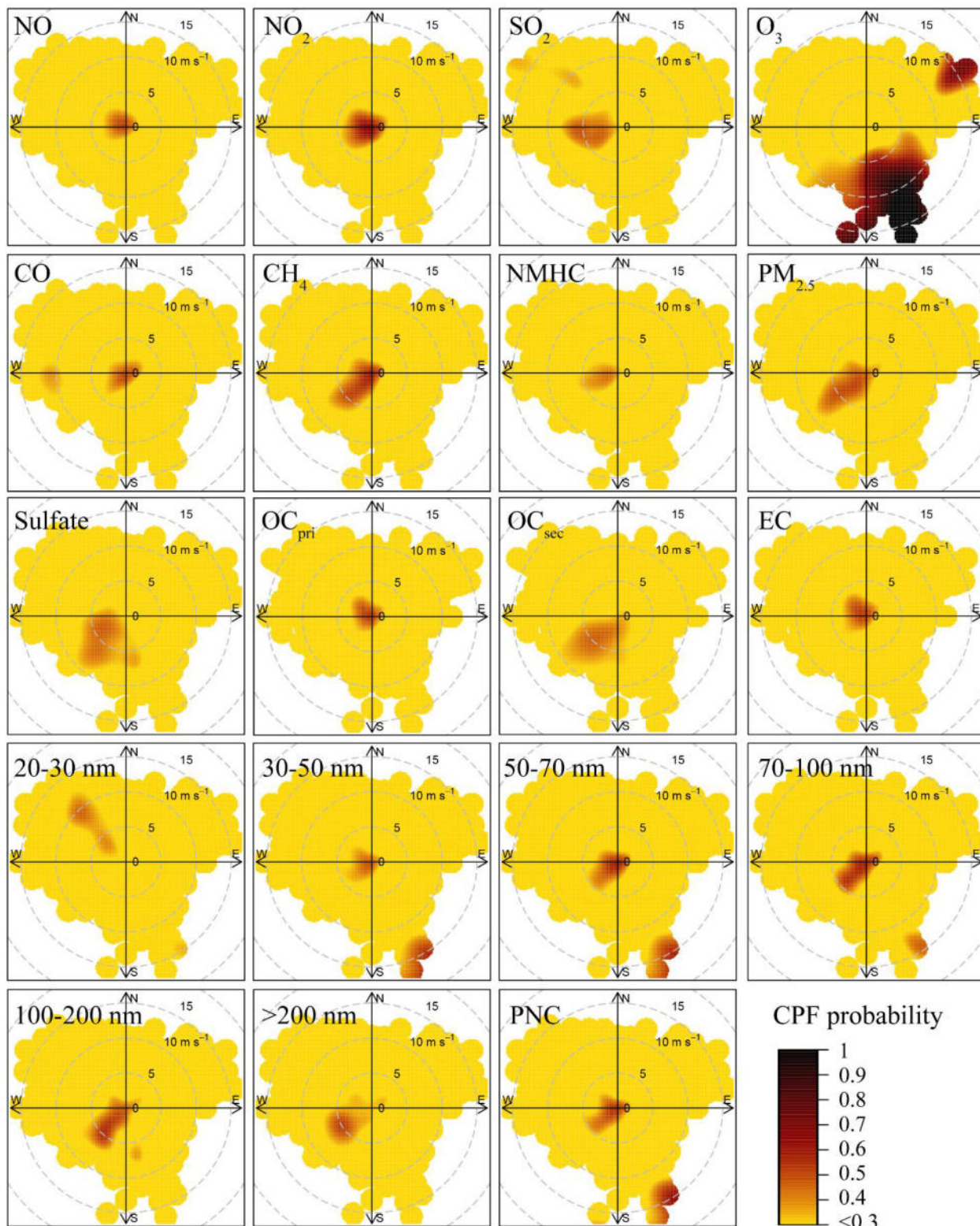
Figure 5. CBPF for pollutants measured at QC. CPF criteria: data from the whole sampling campaign; selected threshold: concentrations> 75th percentile.
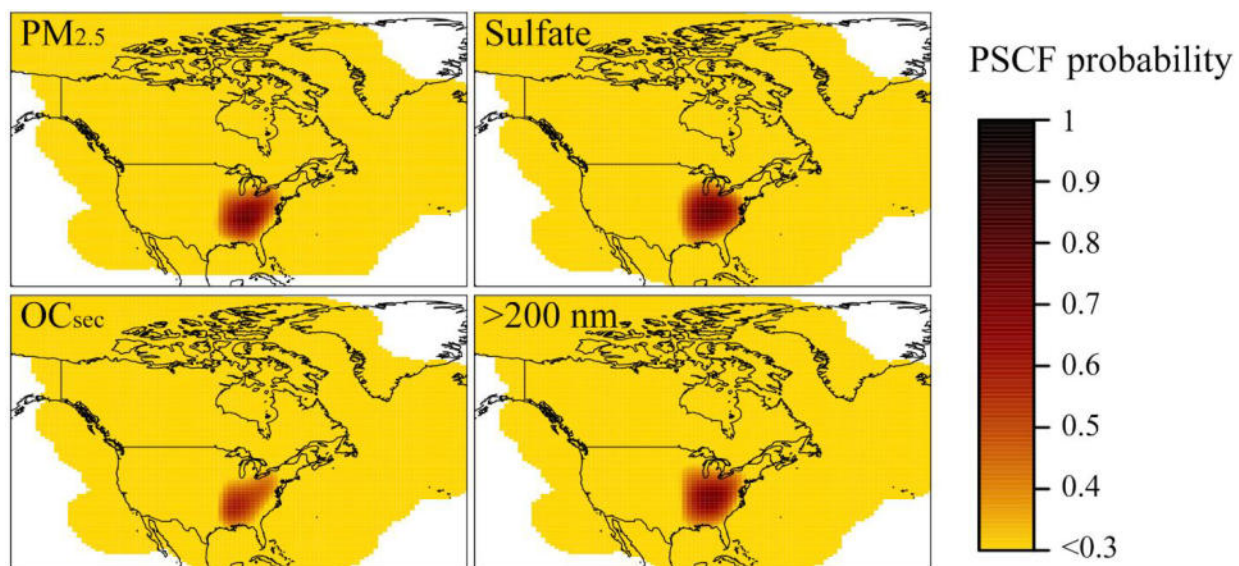
Figure 6. Smoothed PSCF maps for pollutants measured at QC during the whole sampling campaign. Selected threshold for PSCF: concentrations> 75th percentile.